# Mass transfer correlations for nonaqueous phase liquid pool dissolution in saturated porous media

**ARTICLE** *in* WATER RESOURCES RESEARCH · FEBRUARY 1999

Impact Factor: 3.71 · DOI: 10.1029/1998WR900053

WATER RESOURCES RESEARCH, VOL. 35, NO. 2, PAGES 449–459, FEBRUARY 1999

# Mass transfer correlations for nonaqueous phase liquid pool dissolution in saturated porous media

Tae-Joon Kim and Constantinos V. Chrysikopoulos

Department of Civil and Environmental Engineering, University of California, Irvine

**Abstract.** Correlations describing the rate of interface mass transfer from single-component nonaqueous phase liquid (NAPL) pools in saturated subsurface formations are developed. A three-dimensional contaminant transport model is employed to obtain overall mass transfer coefficients computed from concentration gradients at the NAPL-water interface. The model assumes that the porous medium is homogeneous, the interstitial fluid velocity is steady, and the dissolved solute may sorb under local equilibrium conditions. Furthermore, it is assumed that the dissolved concentration along the NAPL-water interface is equal to the solubility concentration. Power law correlations relate the overall Sherwood number to the appropriate overall Peclet numbers. Both rectangular and elliptic/circular source geometries are considered. The proposed relationships are fitted to numerically determined mass transfer coefficients, and the correlation coefficients are determined by nonlinear least squares regression. Good agreement between predicted and available experimentally determined overall mass transfer coefficients is observed.

## 1. Introduction

Groundwater contamination by nonaqueous phase liquids (NAPLs), such as petroleum hydrocarbons and organic solvents, has been a growing public concern, because groundwater is a major and, in some parts of the world, the only source of freshwater supply. Introduction of NAPLs into a groundwater system can occur from discharged industrial wastes, leaking storage tanks, and hazardous chemical spills. During NAPL migration through an unsaturated zone, a substantial portion of the NAPL is trapped in aquifer pore spaces by capillary forces in the form of ganglia or blobs [*Schwille*, 1988]. Upon reaching the saturated zone, a NAPL with density smaller than the density of water will form a floating pool on the water table, whereas a NAPL with density greater than the density of water will keep migrating downward until an impermeable layer is encountered, where a pool may be formed [*Seagren et al*., 1994; *Chrysikopoulos*, 1995].

Typical interfacial contact areas of NAPL pools with groundwater are smaller than the corresponding areas of ganglia, and thus pools dissolve substantially slower than ganglia and often are long-lasting sources of contamination [*Anderson et al*., 1992]. The dissolution of NAPLs in the subsurface is governed by mass transfer processes. The significance of mass transfer rate on fate and transport of NAPLs in subsurface formations has been extensively investigated for both ganglia [*Miller et al*., 1990; *Powers et al*., 1991, 1992; *Abriola et al*., 1993; *Geller and Hunt*, 1993; *Illangasekare et al*., 1995] and pools [*Johnson and Pankow*, 1992; *Chrysikopoulos et al*., 1994; *Holman and Javandel*, 1996; *Lee and Chrysikopoulos*, 1995, 1998].

Mathematical models for mass transfer at the NAPL-water interface often adopt the assumption that implies that thermodynamic equilibrium is instantaneously approached when mass transfer rates at the NAPL-water interface are much faster than the advective-dispersive transport of the dissolved NAPLs away from the interface [*Pinder and Abriola*, 1986; *Holman and Javandel*, 1996]. Therefore the solubility concentration is often employed as an appropriate concentration boundary condition specified at the interface. Some experimental column studies justified the above equilibrium assumption for residual NAPL dissolution. *Borden and Kao* [1992] and *Borden and Piwoni* [1992] conducted residual NAPL dissolution experiments and observed that the equilibrium model reasonably fit experimental results at the laboratory scale. *Miller et al*. [1990] observed equilibrium effluent concentrations at the end of a packed column. Other studies have also verified the solubility concentration condition between NAPL and aqueous phases at typical groundwater velocities in homogeneous porous media contaminated by small NAPL blobs [*van der Waarden et al*., 1971; *Fried et al*., 1979].

Several field experiments indicated that concentrations of dissolved NAPLs in groundwater are often significantly below equilibrium levels [*Schwille*, 1975; *Mackay et al*., 1985]. Equilibrium concentrations in subsurface environments are rarely achieved, because regions heavily contaminated with trapped NAPLs often exhibit reduced formation permeabilities. Such regions are preferentially bypassed by groundwater [*Wilson et al*., 1988]. Interface mass transfer limitations are also attributed to nonuniform groundwater flow caused by aquifer heterogeneities [*Powers et al*., 1991; *Mayer and Miller*, 1996] or are due to the presence of a capillary fringe [*Anderson et al*., 1992].

The equilibrium aqueous solubility condition at the NAPL-water interface is generally a good assumption for typical groundwater velocities. It should be noted that NAPL pools are continuous and nearly saturated zones of NAPLs that are relatively thin compared with a typical aquifer thickness. Furthermore, vertical dissolution zones are often much smaller than the vertical scale of aquifer heterogeneity. Consequently, the vertical dissolution zone within an aquifer can be assumed as relatively homogeneous [*Johnson and Pankow*, 1992]. Furthermore, mass transfer limitations at the NAPL-water inter-



Paper number 1998WR900053.
0043-1397/99/1998WR900053$09.00

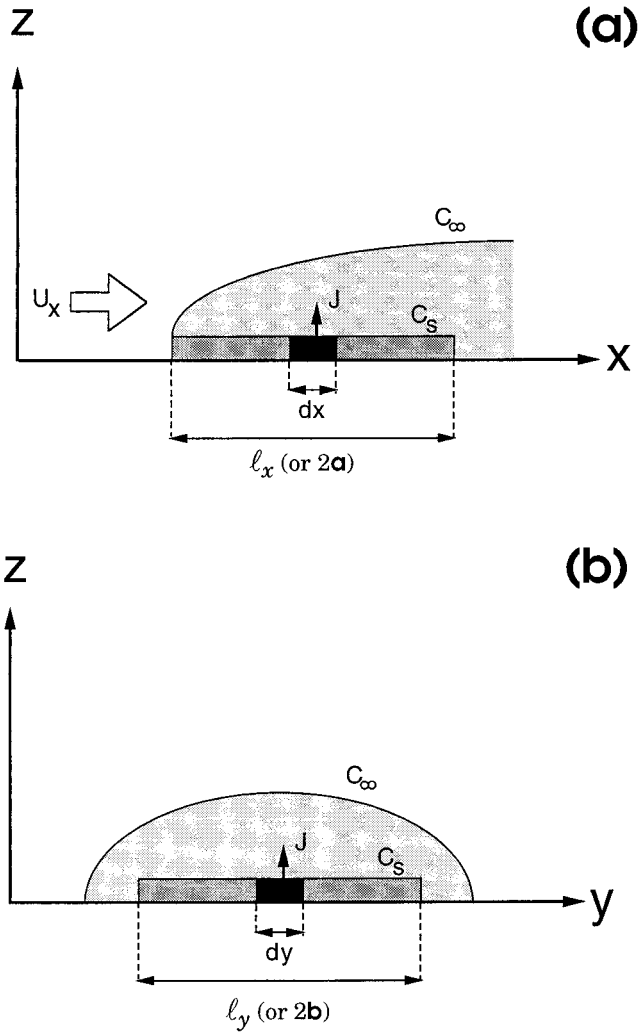


**Figure 1.** Schemetic illustrations of the (a) $xz$ and (b) $yz$ cross sections of a dissolved nonaqueous phase liquid (NAPL) concentration boundary layer. The local mass flux is perpendicular to the NAPL pool surface.

face occur in the presence of irregularly distributed NAPL pools, where adoption of the solubility condition most likely leads to overestimation of NAPL pool dissolution [*Holman and Javandel*, 1996].

In this paper we develop overall mass transfer correlations for the rate of interface mass transfer from single-component NAPL pools in saturated, homogeneous porous media. The correlations relate a dimensionless mass transfer coefficient, i.e., a Sherwood number, to appropriate Peclet numbers. A three-dimensional transport model describing contaminant migration originating from the dissolution of NAPL pools is utilized for numerical estimation of overall mass transfer coefficients. Rectangular, elliptic, and circular NAPL pool shapes are considered in this work. The correlation coefficients are determined using nonlinear least squares regression by fitting the correlations to numerically determined mass transfer coefficients. Predictions based on the mass transfer correlation developed here for rectangular NAPL pools compare favorably with available experimental data.

## 2. Theory

### 2.1. NAPL Dissolution

As a NAPL pool dissolves into an aqueous phase, a concentration boundary layer is developed over the NAPL-water interface. The mass leaving from the NAPL pool into the aqueous interstitial fluid within a saturated porous formation is described by the following mass flux relationship [*Chrysikopoulos et al.*, 1994]:

$$J(t, x, y) = -\mathcal{D}_e \frac{\partial c(t, x, y, 0)}{\partial z}$$

$$= k(t, x, y)[c_s - c(t, x, y, \infty)], \quad (1)$$

where $J(t, x, y)$ is the local mass flux perpendicular to the NAPL pool; $c(t, x, y, z)$ is the aqueous phase contaminant concentration; $c_s$ is the solubility concentration of the organic liquid; $\mathcal{D}_e = \mathcal{D}/\tau$ is the effective molecular diffusion coefficient in the porous medium (where $\mathcal{D}$ is the molecular diffusion coefficient and $\tau \geq 1$ is the tortuosity coefficient); $k(t, x, y)$ is the local mass transfer coefficient dependent on time and location on the NAPL-water interface; $x$, $y$, and $z$ are the spatial coordinates in the longitudinal, lateral, and vertical directions, respectively; and $t$ is time. Note that the NAPL-water interface is located at $z = 0$, and $z \to \infty$ corresponds to any location above the concentration boundary layer (see Figure 1). The concentration along the interface is assumed constant and equal to the solubility concentration, $c(t, x, y, 0) = c_s$. For the case where the background concentration is constant with respect to time and space, for notational convenience, $c(t, x, y, \infty)$ is replaced by $c_b$, the constant background (free stream) aqueous phase concentration. The first formulation in (1) represents the diffusive mass flux into the boundary layer at the NAPL-water interface given by Fick's law, whereas the latter formulation in (1) represents the convective mass transfer flux. Convective mass transfer occurs when $c(t, x, y, 0) \neq c(t, x, y, \infty)$, and is analogous to Newton's law of cooling [*Bird et al.*, 1960, p. 267]. Relationship (1) implies that dissolution at a NAPL-water interface is limited only by the mass transfer of the dissolved solute.

In view of (1) the appropriate expression for the local mass transfer coefficient is given by

$$k(t, x, y) = \frac{-\mathcal{D}_e}{c_s - c_b} \frac{\partial c(t, x, y, 0)}{\partial z}. \quad (2)$$

Relationship (2) implies that the local mass transfer coefficient is proportional to the gradient of the contaminant concentration at the NAPL-water interface. The time required for complete pool dissolution is much longer than the contact time between the pool and the flowing groundwater [*Johnson and Pankow*, 1992; *Seagren et al.*, 1994]. Therefore, in this work, local mass transfer coefficients are estimated at steady state conditions. The time invariant local mass transfer coefficient is denoted by $\hat{k}(x, y)$. Because the local mass transfer coefficient at a specific location is usually not an easy parameter to determine with precision, in mathematical models of contaminant transport $\hat{k}(x, y)$ is often replaced by a time invariant overall (average) mass transfer coefficient $k^*$, for the entire pool, expressed as [*Incropera and DeWitt*, 1990, p. 313; *Chrysikopoulos and Lee*, 1998]

$$k^* = \frac{1}{A} \int_A \hat{k}(x, y)\, d\mathbf{A}, \quad (3)$$

**Table 1.** Correlations for Residual Nonaqueous Phase Liquid Dissolution

| Correlation* | Valid Conditions | Reference |
|---|---|---|
| $Sh^\circ = 340\ Re^{0.71}\theta_n^{0.87}(x/\bar{d}_p)^{-0.31}$ | $0.0012 \le Re \le 0.021,\ 0 \le \theta_n \le 0.04,\ 1.4 \le x/\bar{d}_p \le 180$ | *Imhoff et al.* [1994] |
| $Sh^\circ = 425\ Re^{0.75}\theta_n^{0.60}$ | $0.0015 < Re < 0.1,\ 0.016 < \theta_n < 0.07$ | *Miller et al.* [1990] |
| $Sh^\circ = 1240\ Re^{0.75}\theta_n^{0.60}$ | $0.1 < Re < 0.2,\ 0.02 < \theta_n < 0.03$ | *Parker et al.* [1991] |
| $Sh^\circ = 0.55 + 0.25\ Pe^{1.5}$ | $0.5 < Pe < 100,$ | *Pfannkuch* [1984] |
| $Sh^\circ = 57.7\ Re^{0.61}\ \bar{d}_p^{0.64}\ \Psi_i^{0.41}$ | $0.012 < Re < 0.2,\ \theta_n =$ constant | *Powers et al.* [1992] |

*The Sherwood number is defined as $Sh^\circ = K\bar{d}_p^2/\mathcal{D}$ (where $K = k^\circ a_T$ is the mass transfer rate coefficient, $k^\circ$ is the mass transfer coefficient for ganglia, $a_T$ is the specific interfacial area between the immiscible phases; and $\bar{d}_p$ is the mean particle diameter); the Reynolds number for these correlations is defined as $Re = U_x\bar{d}_p/\nu$ (where $U_x$ is the Darcy flux and $\nu$ is the kinematic viscosity of water); $x/\bar{d}_p$ is the dimensionless distance into the region of residual NAPL; $\theta_n$ is the NAPL volumetric content, and $\Psi_i$ is the uniformity index that represents a grain size distribution.

where $A$ is the surface area of the NAPL pool and $d\mathbf{A}$ is a differential surface area. In this work, $k^*$ is numerically calculated by simply dividing the sum of the estimated time independent local mass transfer coefficients at the nodal points of the entire pool surface by the total number of nodal points used.

A useful application of the time invariant overall mass transfer coefficients is the evaluation of the overall mass transfer rate at a NAPL-water interface, which can be obtained by multiplying the overall mass flux $J^*$ by the entire surface area of the pool $A$ as follows:

$$N = AJ^* = Ak^*[c_s - c_b], \tag{4}$$

where $N$ is the overall mass transfer rate from the NAPL pool into groundwater flow. This mass transfer rate expression has been used in numerous engineering applications, including the NAPL pool dissolution in porous formations [*Lee and Chrysikopoulos*, 1998], evaporation rate of a water pool [*Incropera and DeWitt*, 1996, p. 365], and dissolution of a soluble plate in laminar flow [*Weber and DiGiano*, 1996, p. 202], to mention a few.

### 2.2. Mass Transfer Correlations

Various empirical power law relations (correlations) of dimensionless quantities have been developed to describe the dissolution of residual NAPLs in packed beds in the form of spheres and cylinders [*Pfannkuch*, 1984; *Miller et al*., 1990; *Parker et al*., 1991; *Powers et al*., 1991, 1992; *Geller and Hunt*, 1993; *Abriola et al*., 1993]. These correlations relate dimensionless parameters such as the Reynolds number, Schmidt number, Peclet number, and/or NAPL residual saturation to a dimensionless mass transfer rate coefficient (the Sherwood number). Each dimensionless parameter is a combination of several physical properties of the system. The Reynolds number is a measure of the ratio of the inertia force to the viscous force on a fluid element. The Schmidt number represents the ratio of the eddy momentum dispersivity to molecular diffusion. The Peclet number is the ratio of advective to diffusive mass transport in the concentration boundary layer. The Sherwood number is defined as the ratio of interface mass transfer resistance to molecular diffusion resistance and physically represents the dimensionless concentration gradient at the interface.

Several mass transfer correlations applicable to residual NAPL dissolution are presented in Table 1. All correlations have similar structure, consisting of a leading coefficient and power law forms of the dimensionless parameters used. These correlations account for the NAPL volumetric fraction and are developed for steady state flow conditions in one-dimensional soil columns. The correlations are dependent on blob shape and size, interstitial velocity, and/or length of the zone exposed to residual NAPLs. Note that the length scale associated with the correlations of Table 1 is equal to the mean particle diameter $\bar{d}_p$ of the solid matrix.

## 3. Transport Model

The transient contaminant transport from a dissolving NAPL pool denser than water in a three-dimensional homogeneous porous medium under steady state uniform flow conditions, assuming that the dissolved organic does not decay and is sorbing under local equilibrium conditions, is governed by [*Chrysikopoulos*, 1995]

$$R\frac{\partial c(t,x,y,z)}{\partial t} = D_x\frac{\partial^2 c(t,x,y,z)}{\partial x^2} + D_y\frac{\partial^2 c(t,x,y,z)}{\partial y^2} + D_z\frac{\partial^2 c(t,x,y,z)}{\partial z^2} - U_x\frac{\partial c(t,x,y,z)}{\partial x}, \tag{5}$$

where $U_x$ is the average unidirectional interstitial fluid velocity; $R = 1 + K_d\rho/\theta$ is the dimensionless retardation factor for linear, reversible, instantaneous sorption; $K_d$ is the partition or distribution coefficient; $\rho$ is the bulk density of the solid matrix; $\theta$ is the porosity of the porous medium; and $D_x$, $D_y$, and $D_z$ are the longitudinal, transverse, and vertical hydrodynamic dispersion coefficients, respectively, defined as [*Bear and Verruijt*, 1987, p. 164]

$$D_x = \alpha_L U_x + \mathcal{D}_e, \tag{6a}$$

$$D_y = \alpha_T U_x + \mathcal{D}_e, \tag{6b}$$

$$D_z = \alpha_V U_x + \mathcal{D}_e, \tag{6c}$$

where $\alpha_L$, $\alpha_T$, and $\alpha_V$ are the longitudinal, transverse, and vertical dispersivities, respectively.

For a rectangular-shaped stagnant NAPL pool, as shown in Figure 2a, the appropriate initial and boundary conditions are

$$c(0,x,y,z) = 0, \tag{7}$$

$$c(t,\pm\infty,y,z) = 0, \tag{8}$$

$$c(t,x,\pm\infty,z) = 0, \tag{9}$$

$$c(t,x,y,0) = c_s \qquad x,y \in \mathcal{R}_{(r)}, \tag{10a}$$

$$\frac{\partial c(t,x,y,0)}{\partial z} = 0 \qquad x,y \notin \mathcal{R}_{(r)}, \tag{10b}$$

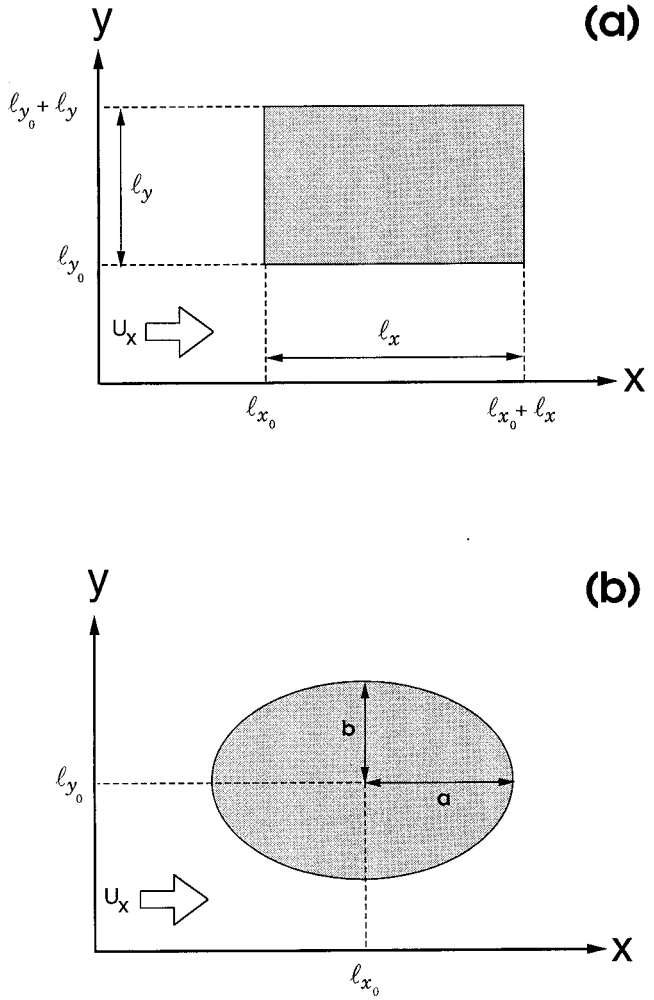


**Figure 2.** Plan views at $z = 0$ of (a) a rectangular dense nonaqueous phase liquid (DNAPL) pool with dimensions $\ell_x \times \ell_y$ and pool origin at $x = \ell_{x_o}$, $y = \ell_{y_o}$ and (b) an elliptic DNAPL pool with major semiaxis $a$ and minor semiaxis $b$ and a pool center located at $x = \ell_{x_o}$, $y = \ell_{y_o}$. The unidirectional groundwater velocity $U_x$ and origin of the corresponding Cartesian coordinate system are shown.

$$c(t, x, y, \infty) = 0, \tag{11}$$

where $\mathcal{R}_{(r)}$ is the domain defined by the rectangular NAPL-water interfacial area ($\ell_{x_o} \le x \le \ell_{x_o} + \ell_x$ and $\ell_{y_o} \le y \le \ell_{y_o} + \ell_y$, where $\ell_{x_o}$ and $\ell_{y_o}$ indicate the $x$ and $y$ Cartesian coordinates of the pool origin, respectively, and $\ell_x$ and $\ell_y$ are the pool dimensions in $x$ and $y$ directions, respectively). Source boundary condition (10a) implies that the aqueous concentration is constant over the pool at $z = 0$ and that the NAPL phase is in equilibrium with the water at the interface. Equation (11) represents the contaminant concentration outside the boundary layer.

For a NAPL pool of elliptic shape, as shown in Figure 2b, the appropriate source boundary condition is

$$c(t, x, y, 0) = c_s \qquad x, y \in \mathcal{R}_{(e)}, \tag{12a}$$

$$\frac{\partial c(t, x, y, 0)}{\partial z} = 0 \qquad x, y \notin \mathcal{R}_{(e)}, \tag{12b}$$

where $\mathcal{R}_{(e)}$ is the domain defined by an elliptic NAPL-water interfacial area ($(x - \ell_{x_o})^2/a^2 + (y - \ell_{y_o})^2/b^2 \le 1$, where $a$ and $b$ are the major and minor semiaxes of the elliptic pool, respectively). Because a circular pool with radius $r$ is just a special case of an elliptic pool, the appropriate source boundary condition for a circular pool is obtained by setting $a = b = r$.

It is generally more convenient to work with models written in dimensionless variables. Hence, by introducing the following dimensionless definitions:

$$C = \frac{c}{c_s}, \tag{13}$$

$$X = \frac{x}{\ell_c}, \tag{14}$$

$$Y = \frac{y}{\ell_c}, \tag{15}$$

$$Z = \frac{z}{\ell_c}, \tag{16}$$

$$T = \frac{U_x t}{\ell_c}, \tag{17}$$

$$Pe_X = \frac{U_x \ell_c}{D_x}, \tag{18}$$

$$Pe_Y = \frac{U_x \ell_c}{D_y}, \tag{19}$$

$$Pe_Z = \frac{U_x \ell_c}{D_z}, \tag{20}$$

where $\ell_c$ is the square root of the pool area ($(\ell_x \ell_y)^{1/2}$ or $(\pi ab)^{1/2}$) and is used here as a characteristic length, model equations (5) and (7)–(12) are transformed to yield

$$R \frac{\partial C(T, X, Y, Z)}{\partial T} = \frac{1}{Pe_X} \frac{\partial^2 C(T, X, Y, Z)}{\partial X^2} + \frac{1}{Pe_Y} \frac{\partial^2 C(T, X, Y, Z)}{\partial Y^2} + \frac{1}{Pe_Z} \frac{\partial^2 C(T, X, Y, Z)}{\partial Z^2} - \frac{\partial C(T, X, Y, Z)}{\partial X}, \tag{21}$$

$$C(0, X, Y, Z) = 0, \tag{22}$$

$$C(T, \pm\infty, Y, Z) = 0, \tag{23}$$

$$C(T, X, \pm\infty, Z) = 0, \tag{24}$$

$$C(T, X, Y, 0) = 1 \qquad X, Y \in \mathcal{R}_{(r)}, \tag{25a}$$

$$\frac{\partial C(T, X, Y, 0)}{\partial Z} = 0 \qquad X, Y \notin \mathcal{R}_{(r)}, \tag{25b}$$

$$C(T, X, Y, \infty) = 0, \tag{26}$$

$$C(T, X, Y, 0) = 1 \qquad X, Y \in \mathcal{R}_{(e)}, \tag{27a}$$

$$\frac{\partial C(T, X, Y, 0)}{\partial z} = 0 \qquad X, Y \notin \mathcal{R}_{(e)}, \tag{27b}$$

where the dimensionless $\mathcal{R}_{(r)}$ is expressed as $\ell_{x_o}/\ell_c \le X \le (\ell_{x_o} + \ell_x)/\ell_c$, $\ell_{y_o}/\ell_c \le Y \le (\ell_{y_o} + \ell_y)/\ell_c$, and $\mathcal{R}_{(e)}$ is expressed as $(X - \ell_{x_o}/\ell_c)^2/a^2 + (Y - \ell_{y_o}/\ell_c)^2/b^2 \le \ell_c^{-2}$. It

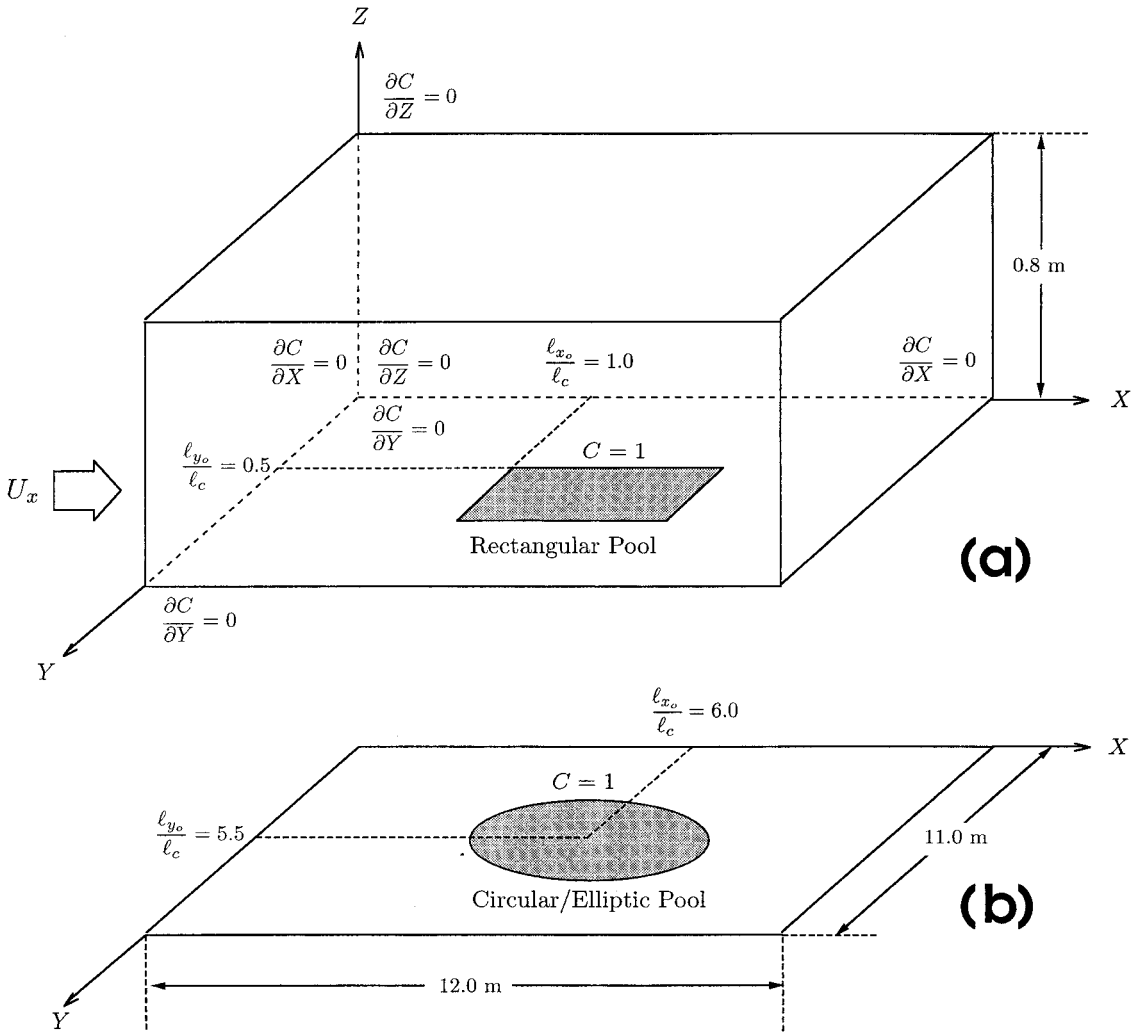


**Figure 3.** Schemetic illustration of the three-dimensional numerical domain showing the (a) rectangular and (b) elliptic/circular DNAPL pools together with the appropriate boundary conditions.

should be noted that conditions (25a) and (25b) correspond to the case of a rectangular pool, whereas conditions (27a) and (27b) represent an elliptic/circular pool. It should be noted that source boundary conditions (25a) and (27a) are independent of $c_s$; therefore the dimensionless equations (21)–(27) can be used regardless of the contaminant type. Similarly, the local mass transfer coefficient (equation (2)) is transformed as follows:

$$k(T, X, Y) = -\frac{\mathcal{D}_e}{\ell_c}\frac{\partial C(T, X, Y, 0)}{\partial Z}. \tag{28}$$

In view of the preceding equation, the dimensionless form of the local mass transfer coefficient, i.e., the local Sherwood number, is given by

$$Sh(T, X, Y) = \frac{k(T, X, Y)\ell_c}{\mathcal{D}_e} = -\frac{\partial C(T, X, Y, 0)}{\partial Z}. \tag{29}$$

For the time invariant local mass transfer coefficient $\hat{k}(x, y)$, the corresponding time invariant local Sherwood number is denoted by $\widehat{Sh}(X, Y)$. Accordingly, the time invariant overall Sherwood number is defined as

$$Sh^* = \frac{k^*\ell_c}{\mathcal{D}_e} = \frac{1}{A}\int_A \widehat{Sh}(X, Y)\, d\mathbf{A}. \tag{30}$$

## 4. Numerical Solution

The three-dimensional mathematical model presented by (21) is solved numerically by an alternating direction implicit (ADI) finite difference scheme. The unconditionally stable ADI algorithm for three-dimensional transient partial differential equations is described by *Huyakorn and Pinder* [1983, p. 358]. The ADI algorithm leads to a set of algebraic equations that form a tridiagonal matrix which is solved by the highly efficient Thomas algorithm [*Wang and Anderson*, 1982, p. 96].

Numerical simulations are performed to estimate profiles of dissolved NAPL concentrations for various interstitial velocities, pool dimensions, and pool geometries. A separate numerical code for each pool geometry considered is developed. The numerical domain as well as the corresponding boundary conditions used in this work are schematically illustrated in Figure 3. Zero-concentration gradient boundary conditions are applied to all outer boundaries of the numerical domain, and a

constant dimensionless concentration boundary condition (equation (25a)) as shown in Figure 3a or (27a) shown in Figure 3b is applied at the pool-water interface. In order to avoid numerical oscillations, the dimensionless nodal separation distances and numerical time steps are selected so that the following criteria are satisfied [*Hoffman*, 1992, p. 672; *Schincariol et al*., 1994]:

$$Pe_X \Delta X \leq 2 \qquad Pe_Y \Delta Y \leq 2 \qquad Pe_Z \Delta Z \leq 2, \tag{31}$$

$$\max\left(\frac{\Delta T}{\Delta X}, \frac{\Delta T}{\Delta Y}, \frac{\Delta T}{\Delta Z}\right) \leq 1, \tag{32}$$

where $\Delta X$, $\Delta Y$, and $\Delta Z$ are the nondimensionalized distances between the nodes in the $X$, $Y$, and $Z$ spatial coordinates, respectively, and $\Delta T$ is the dimensionless numerical time step. The time step size is determined by (32) according to the selected dimensionless nodal separation distances. The numerical codes developed were consistently run until the simulated dissolved concentration profiles become time independent, because in this study the local mass transfer coefficients are calculated at steady state conditions.

## 5. Development of Mass Transfer Correlations

### 5.1. Simulation Conditions

The interstitial fluid velocities employed for model simulations are 0.3, 0.5, 0.7, and 1.0 m/d, because equilibrium mass transfer conditions may exist at interstitial fluid velocities of up to 1.0 m/d [*Powers et al*., 1991]. The dimensionless retardation factor $R$ is arbitrarily set to 1.0, because at steady state conditions concentration profiles for a nondecaying solute are no longer dependent on $R$ [*Chrysikopoulos et al*., 1994]. The dispersion coefficients $D_x$, $D_y$, and $D_z$ are chosen in the ranges 2.5–8.3 $\times 10^{-2}$ m$^2$/h; 2.5–8.3 $\times 10^{-3}$ m$^2$/h; and 2.5–8.3 $\times 10^{-3}$ m$^2$/h, respectively. The corresponding Peclet numbers are obtained from (18)–(20). A total of 121 different rectangular pools with dimensions $\ell_x \times \ell_y$ in the range from 5.0 $\times$ 5.0 m to 10.0 $\times$ 10.0 m and 121 different elliptic/circular pools with semiaxes $a \times b$ in the range 2.5 $\times$ 2.5 m to 5.0 $\times$ 5.0 m are examined in this work. Overall Sherwood numbers are obtained from (30) for various Peclet numbers, pool sizes, and pool shapes.

### 5.2. Overall Mass Transfer Correlations

**5.2.1. Rectangular pools.** For a DNAPL pool located on an impermeable layer, a concentration boundary layer is developed over the NAPL-water interface due to concentration differences. The possible formation of a groundwater velocity boundary layer near the surface of the NAPL pool is ignored, because the velocity boundary layer is assumed to be smaller than the concentration boundary layer. Consequently, the groundwater flow is assumed to be uniform within the concentration boundary layer, and fluid properties that determine the velocity boundary layer such as fluid dynamic viscosity and density of both groundwater and NAPLs do not contribute to the formation of a concentration boundary layer.

The correlation models are obtained by use of the Buckingham pi theorem, which states that the smallest number of dimensionless groups representing a system is determined by the difference between the number of associated variables and the number of basic dimensions of the variables [*Bird et al*., 1960; *Perry et al*., 1984; *Weber and DiGiano*, 1996]. For a two-dimensional NAPL pool with a NAPL-water interface on the $xy$ plane, $U_x$, $D_x$, and $D_y$ are very important transport parameters. Because there is no fluid motion on the NAPL pool surface, dissolution from the pool surface in the $z$ direction is controlled by the effective molecular diffusion. This is an appropriate assumption when the no-slip boundary condition is valid [*Bear and Verruijt*, 1987]. Dispersion in the $z$ direction affects the thickness of the concentration boundary layer, but it is assumed not to have a direct impact on mass transfer at the NAPL-water interface. The contact time between the NAPL pool and the flowing groundwater is significantly affecting the concentration gradient at the NAPL-water interface [*Johnson and Pankow*, 1992; *Chrysikopoulos*, 1995], so pool length and size must be considered in the development of the mass transfer correlations. The selected fundamental variables that affect mass transfer from a single-component rectangular NAPL pool are the interstitial groundwater velocity, effective molecular diffusion, hydrodynamic dispersion coefficients in $x$ and $y$ directions, pool length in both $x$ and $y$ directions, and the characteristic length of the pool, which is equal to the square root of the NAPL-water interface area. The overall mass transfer coefficient of a single-component rectangular NAPL pool is expressed by the following functional relationship:

$$k^* = f[U_x, \mathcal{D}_e, D_x, D_y, \ell_x, \ell_y, \ell_c], \tag{33}$$

where $f$ is an arbitrary function.

There are eight dimensional variables in (33), and their fundamental dimensions are length ($L$) and time ($t$). Therefore the minimum number of dimensionless groups needed to characterize the overall mass transfer coefficient is six. Relationship (33) can be rearranged into

$$\phi[\Pi_1, \Pi_2, \cdots, \Pi_6] = 0, \tag{34}$$

where each $\Pi$ is an independent dimensionless product of some of the dimensional variables of the system considered and $\phi$ is an arbitrary function. Dimensional analysis yields the following $\Pi$ terms:

$$\Pi_1 = \frac{k^*}{U_x}, \tag{35}$$

$$\Pi_2 = \frac{D_x}{\mathcal{D}_e}, \tag{36}$$

$$\Pi_3 = \frac{D_y}{\mathcal{D}_e}, \tag{37}$$

$$\Pi_4 = \frac{U_x \ell_x}{\mathcal{D}_e}, \tag{38}$$

$$\Pi_5 = \frac{U_x \ell_y}{\mathcal{D}_e}, \tag{39}$$

$$\Pi_6 = \frac{U_x \ell_c}{\mathcal{D}_e}. \tag{40}$$

The overall Sherwood number can be expressed by the following product of $\Pi$ terms:

$$Sh^* = \Pi_1 \Pi_6 = \frac{k^* \ell_c}{\mathcal{D}_e}. \tag{41}$$

Similarly, the overall Peclet numbers, $Pe^*_{x(r)}$ and $Pe^*_{y(r)}$, can be obtained from the following combinations of $\Pi$ terms

$$Pe^*_{x(r)} = \frac{\Pi_4}{\Pi_2} = \frac{U_x \ell_x}{D_x}, \quad (42)$$

$$Pe^*_{y(r)} = \frac{\Pi_5}{\Pi_3} = \frac{U_x \ell_y}{D_y}, \quad (43)$$

where subscript r designates a rectangular pool. It should be noted that the characteristic length scale $\ell_c$ is related to the size of the pool rather than to the mean grain diameter of the solid matrix, $\bar{d}_p$, which is often employed in mass transfer correlations for residual NAPL blobs (see Table 1).

The proposed mass transfer correlation for rectangular NAPL pools under uniform flow conditions can be described by a power law model consisting of the two directional Peclet numbers and a leading coefficient, as follows:

$$Sh^*_{(r)} = \beta_1 (Pe^*_{x(r)})^{\beta_2} (Pe^*_{y(r)})^{\beta_3}, \quad (44)$$

where $\beta_1$, $\beta_2$, and $\beta_3$ are empirical coefficients to be determined. The nonlinear least squares regression routine (RNLIN) [*International Mathematics and Statistics Libraries*, 1991] is employed to estimate the coefficients $\beta_1$, $\beta_2$, and $\beta_3$ by fitting the nonlinear power law correlation (44) to 484 overall Sherwood numbers computed for 121 different pool dimensions and four different sets of hydrodynamic conditions. The resulting overall mass transfer correlation for rectangular pools is

$$Sh^*_{(r)} = 1.58 (Pe^*_{x(r)})^{0.34} (Pe^*_{y(r)})^{0.43}. \quad (45)$$

This correlation is valid for groundwater velocities in the range from 0.1 to 1.0 m/d. In Figure 4, Sherwood numbers computed by (30) (circles) are compared with those predicted by (45) (lines) as a function of $Pe^*_{x(r)}$ (Figure 4a) and $Pe^*_{y(r)}$ (Figure 4b). Excellent agreement is observed for both cases.

**5.2.2. Elliptic/circular pools.** Following the procedure outlined for the development of the overall mass transfer correlation for rectangular pools, the corresponding overall Peclet numbers for elliptic/circular pools are obtained as follows:

$$Pe^*_{x(e)} = \frac{U_x a}{D_x}, \quad (46)$$

$$Pe^*_{y(e)} = \frac{U_x b}{D_y}, \quad (47)$$

where subscript e refers to an elliptic pool. Furthermore, the proposed overall mass transfer correlation for elliptic/circular pools is given by

$$Sh^*_{(e)} = \gamma_1 (Pe^*_{x(e)})^{\gamma_2} (Pe^*_{y(e)})^{\gamma_3}, \quad (48)$$

where $\gamma_1$, $\gamma_2$, and $\gamma_3$ are empirical coefficients to be determined by nonlinear least squares regression of 484 numerically obtained $Sh^*$ values for 121 different elliptic/circular pools and four different interstitial velocities.

The complete correlation for the case of elliptic/circular pools is given by

$$Sh^*_{(e)} = 1.74 (Pe^*_{x(e)})^{0.33} (Pe^*_{y(e)})^{0.40}, \quad (49)$$

and it is valid for groundwater velocities in the range from 0.1 to 1.0 m/d. Figure 5 illustrates the excellent agreement between Sherwood numbers computed with relationship (30) (circles) and those predicted by correlation (49) (lines) as a function of $Pe^*_{x(e)}$ (Figure 5a) and $Pe^*_{y(e)}$ (Figure 5b).

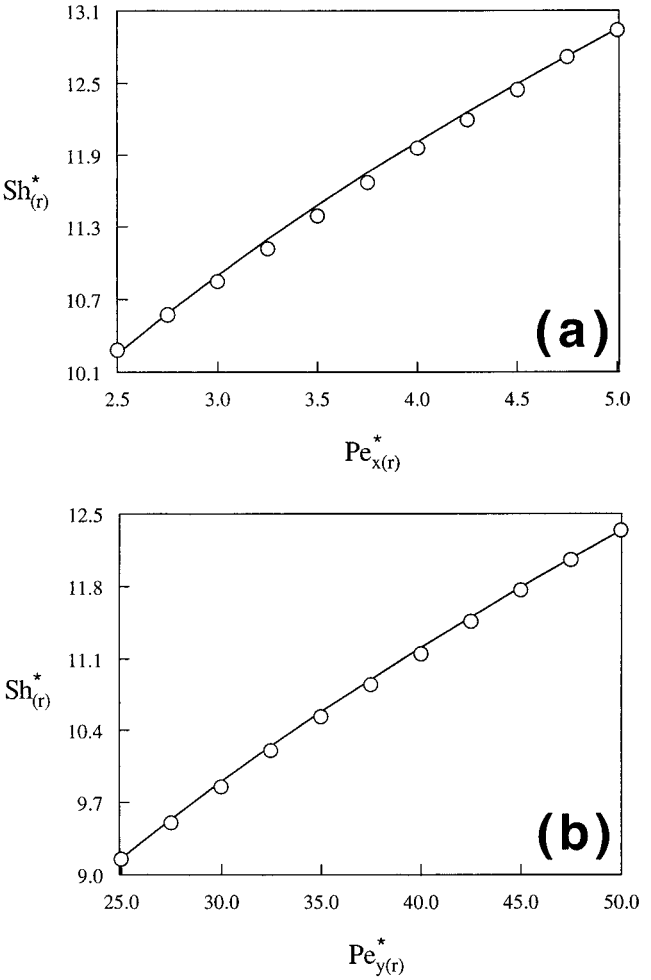


**Figure 4.** Computed (circles) and predicted (lines) overall Sherwood numbers for rectangular pools, as a function of (a) $Pe^*_{x(r)}$ with $Pe^*_{y(r)} = 37.5$ and (b) $Pe^*_{y(r)}$ with $Pe^*_{x(r)} = 3.75$.

### 5.3. Correlation Testing

In order to gain a better understanding of the behavior of the time invariant overall mass transfer coefficient ($k^*$) under different hydrodynamic conditions, two sets of numerical simulations were conducted. For the first set of simulations all system parameters were kept constant except $U_x$. The results are presented in Figure 6a, where it is shown that $k^*$ increases with increasing $U_x$. Consequently, an increase in interstitial velocity leads to enhanced NAPL pool dissolution. It should be noted that the predicted mass transfer coefficients approach an asymptotic value at a relatively low $U_x$. Similar behavior has been observed for residual NAPL dissolution, where the velocity at which the mass transfer coefficients are leveling off is proportional to the degree of NAPL saturation or to the magnitude of the existing NAPL-water interfacial contact area [*Miller et al.*, 1990]. For the second set of simulations all system parameters were kept constant while the dispersivities $\alpha_L/10 = \alpha_T = \alpha_V$ were varied. The results are presented in Figure 6b and indicate that the smaller the dispersivities the larger the overall mass transfer coefficient. Note that increasing aquifer dispersivities leads to a thicker concentration boundary layer and consequently to reduced NAPL pool dissolution. The reason for this is that the concentration boundary layer thickness

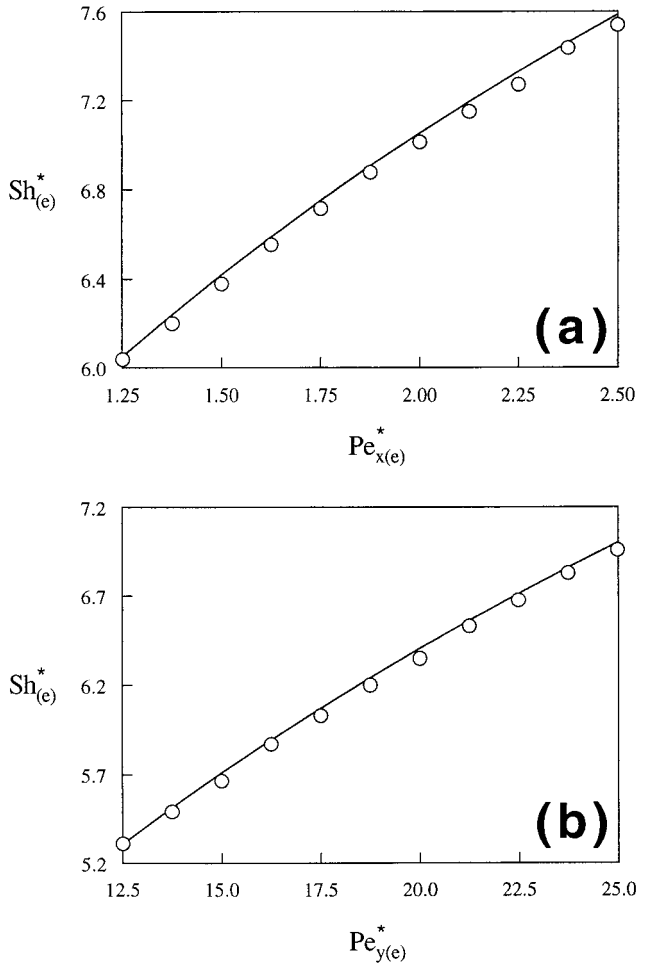


**Figure 5.** Computed (circles) and predicted (lines) overall Sherwood numbers for elliptic/circular pools, as a function of (a) $Pe^*_{x(e)}$ with $Pe^*_{y(e)} = 18.75$ and (b) $Pe^*_{y(e)}$ with $Pe^*_{x(e)} = 1.875$.

is inversely proportional to the mass transfer coefficient [*Miller et al.*, 1990; *Chrysikopoulos and Lee*, 1998].

The effect of $U_x$ and $\alpha_L/10 = \alpha_T = \alpha_V$ on the concentration boundary layer thickness is illustrated in Figure 7. Contours of concentrations originating from the dissolution of a single-component NAPL pool with origin at $x = \ell_{x_o} = 1.0$ m and length $\ell_x = 2.0$ m for two different interstitial velocities ($U_x = 0.5$ and 1.0 m/d) are presented in Figure 7a. Clearly, increasing $U_x$ leads to a thinner concentration boundary layer. Similar concentration contours for two sets of dispersivities ($\alpha_L/10 = \alpha_T = \alpha_V = 0.01$ and 0.03 m) are presented in Figure 7b. It is evident that above the NAPL pool a thinner concentration layer corresponds to the set of smaller dispersivities. Therefore increasing the Peclet numbers by either increasing the interstitial velocity or decreasing the aquifer dispersivities leads to increased mass transfer from the NAPL pool. This result is in perfect agreement with the correlations developed in this work that suggest that the dimensionless mass transfer coefficient (the Sherwood number) increases with increasing Peclet numbers.

The correlation developed in this work for elliptic/circular NAPL pools (equation (49)) is employed to simulate mass transfer coefficients obtained from a circular trichloroethylene (TCE) pool dissolution experiment conducted by *Lee et al.* [1998] in a homogeneous, fully saturated bench scale aquifer under various interstitial velocities ($a = b = 0.038$ m, $\mathcal{D}_e = 1.73 \times 10^{-6}$ m$^2$/h, $\alpha_L = 0.002$ m, and $\alpha_T = \alpha_V = 0.0002$ m). The dispersivities, $\alpha_L$, $\alpha_T$, $\alpha_V$, and the tortuosity required for the evaluation of the effective molecular diffusion, $\mathcal{D}_e$, were obtained from tracer experiments. The values of $k^*$ were determined by fitting the observed steady state TCE concentrations against the analytical solution developed by *Chrysikopoulos* [1995] at three different interstitial velocities. The parameters $Pe^*_{x(e)}$ and $Pe^*_{y(e)}$ required in correlation (49) are calculated from (46) and (47), respectively, and the corresponding mass transfer coefficients are determined with (30). An excellent agreement between predicted and experimentally determined overall mass transfer coefficients is shown in Figure 8.

## 6. Summary

Overall mass transfer correlations for the prediction of interface mass transfer coefficients associated with the dissolution of both rectangular and elliptic/circular NAPL pools in saturated porous media are developed. A nondimensionalized solute transport equation is solved using an ADI finite difference numerical scheme in order to estimate overall mass transfer coefficients for each geometry considered. It is assumed

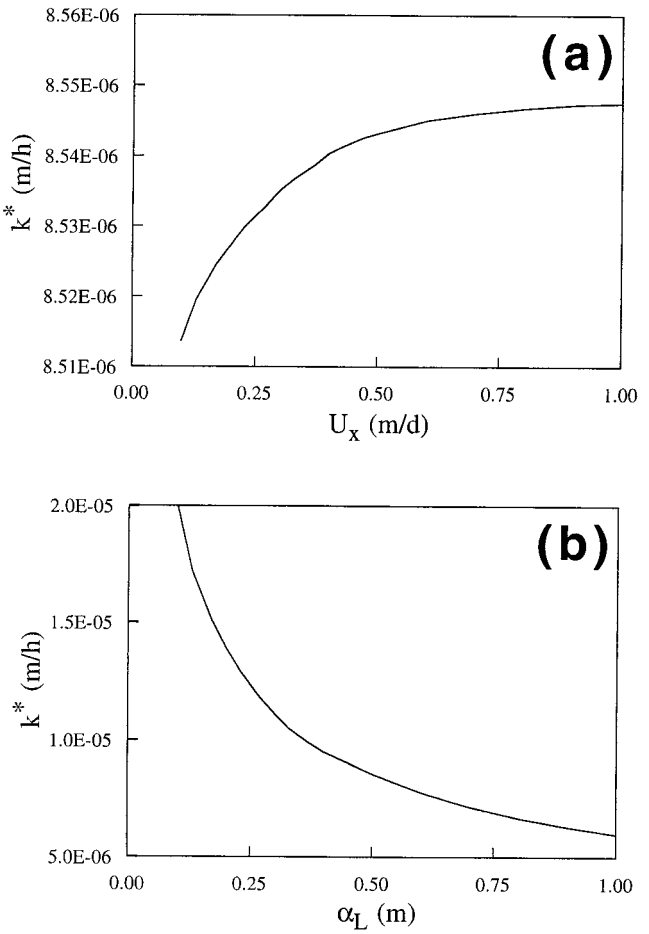


**Figure 6.** Computed overall mass transfer coefficients for a 2.0 × 2.0 m single-component rectangular NAPL pool as a function of (a) $U_x$ with $\alpha_L/10 = \alpha_T = \alpha_V = 0.01$ m and (b) $\alpha_L$ with $U_x = 0.3$ m/d and $\alpha_L/10 = \alpha_T = \alpha_V$.

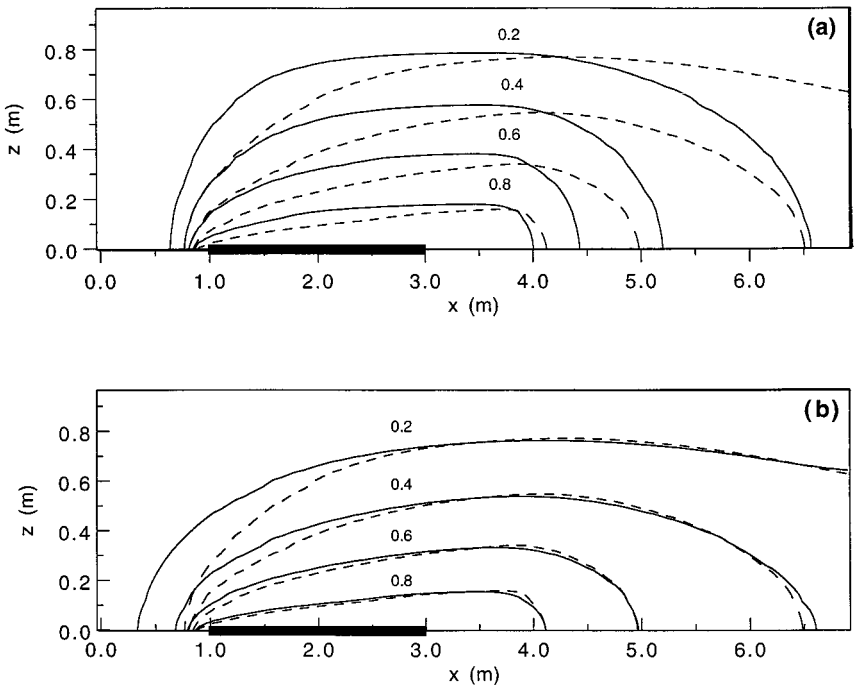


**Figure 7.** Comparison between $x$, $z$ plane concentration contours originating from a single-component NAPL pool computed for (a) $U_x = 1.0$ m/d (dashed lines) and $U_x = 0.5$ m/d (solid lines), and (b) $\alpha_L/10 = \alpha_T = \alpha_V = 0.01$ m (dashed lines) and $\alpha_L/10 = \alpha_T = \alpha_V = 0.03$ m (here $\ell_{x_o} = 1.0$ m and $\ell_x = 2.0$ m).

that the aqueous phase concentration of the dissolved solute adjacent to the NAPL pool is equal to the solubility limit. The correlations developed relate dimensionless overall mass transfer coefficients (Sherwood numbers) to Peclet numbers. The proposed power law correlations are calibrated with overall mass transfer coefficients obtained from numerical simulations. Predictions based on the newly developed mass transfer correlation for elliptic/circular pools are compared with experimentally determined overall mass transfer coefficients. Good agreement between measured and predicted mass transfer coefficients is observed. The correlations presented here can be used to accurately predict the mass transfer coefficients for single-component NAPL pool dissolution in fully saturated subsurface formations with interstitial velocity less than 1.0 m/d.

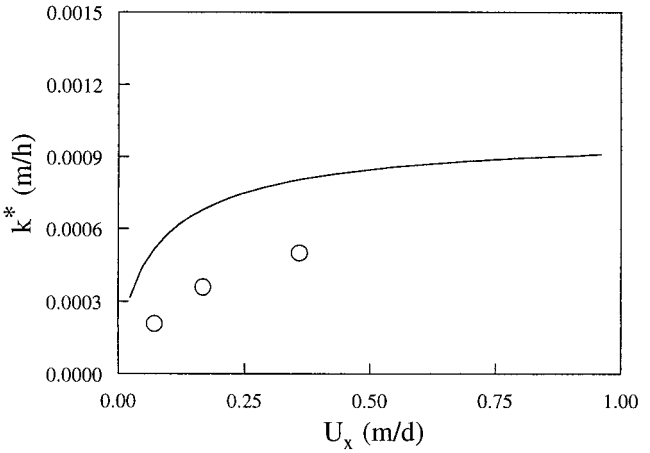


**Figure 8.** Comparison between experimentally determined overall mass transfer coefficients (circles) and those predicted by correlation (49) (line).

## Notation

- $a$ major semiaxis of elliptic pool, $L$.
- $a_T$ specific interfacial area between nonaqueous and aqueous phases per unit volume, $L^2/L^3$.
- $A$ pool surface area, $L^2$.
- $b$ minor semiaxis of elliptic pool, $L$.
- $c$ aqueous phase solute concentration (solute mass/liquid volume), $M/L^3$.
- $c_b$ background (free stream) aqueous phase solute concentration, $M/L^3$.
- $c_s$ single-component aqueous saturation concentration (solubility), $M/L^3$.
- $C$ dimensionless aqueous phase solute concentration defined in equation (13).
- $\bar{d}_p$ mean particle diameter, $L$.
- $d\mathbf{A}$ differential surface area.
- $\mathcal{D}$ molecular diffusion coefficient, $L^2/t$.
- $\mathcal{D}_e$ effective molecular diffusion coefficient, equal to $\mathcal{D}/\tau$, $L^2/t$.
- $D_x$, $D_y$, $D_z$ longitudinal, transverse, and vertical hydrodynamic dispersion coefficients, respectively, $L^2/t$.
- $f$ arbitrary function.
- $J$ local mass flux perpendicular to the NAPL pool, $M/L^2/t$.
- $J^*$ overall mass flux perpendicular to the NAPL pool, $M/L^2/t$.
- $k$ local mass transfer coefficient, $L/t$.
- $\hat{k}$ time invariant local mass transfer coefficient, $L/t$.
- $k^*$ time invariant overall mass transfer coefficient, $L/t$.

$k^\circ$ mass transfer coefficient for ganglia, $L/t$.
$K$ mass transfer rate coefficient for ganglia, $1/t$.
$K_d$ partition coefficient (liquid volume/solid mass), $L^3/M$.
$\ell_c$ characteristic length, equal to $(\ell_x \ell_y)^{1/2}$ or $(\pi ab)^{1/2}$, $L$.
$\ell_x$, $\ell_y$ pool dimensions in $x$ and $y$ directions, $L$.
$\ell_{x_o}$, $\ell_{y_o}$ $x$ and $y$ Cartesian coordinates of the origin of a rectangular pool or the center of an elliptic/circular pool, $L$.
$N$ overall mass transfer rate of the NAPL pool, $M/t$.
$Pe_X$, $Pe_Y$, $Pe_Z$ longitudinal, transverse and vertical Peclet numbers, defined in equations (18), (19), and (20), respectively.
$Pe^*_{x(e)}$, $Pe^*_{y(e)}$ overall Peclet numbers of an elliptic/circular pool in $x$ and $y$ directions, defined in equations (46) and (47), respectively.
$Pe^*_{x(r)}$, $Pe^*_{y(r)}$ overall Peclet numbers of a rectangular pool in $x$ and $y$ directions, defined in equations (42) and (43), respectively.
$R$ dimensionless retardation factor.
$\mathcal{R}_{(e)}$ region defined by an elliptic NAPL-water interfacial area.
$\mathcal{R}_{(r)}$ region defined by a rectangular NAPL-water interfacial area.
$Re$ Reynolds number for residual NAPL dissolution, equal to $U_x \bar{d}_p/\nu$.
$Sh$ local Sherwood number.
$\widehat{Sh}$ time invariant local Sherwood number.
$Sh^*$ time invariant overall Sherwood number.
$Sh^\circ$ Sherwood number for residual NAPL dissolution, equal to $K(\bar{d}_p)^2/\mathcal{D}$.
$t$ time, $t$.
$T$ dimensionless time defined in equation (17).
$\Delta T$ dimensionless numerical time step.
$U_x$ average interstitial velocity, $L/t$.
$x$, $y$, $z$ spatial coordinates in the longitudinal, transverse, and vertical directions, respectively, $L$.
$X$, $Y$, $Z$ dimensionless longitudinal, transverse, and vertical lengths, defined in equations (14), (15), and (16), respectively.
$\Delta X$, $\Delta Y$, $\Delta Z$ nondimensionalized distances between the numerical nodes in $x$, $y$, and $z$ spatial directions, respectively.

**Greek Letters**

$\alpha_L$, $\alpha_T$, $\alpha_V$ longitudinal, transverse, and vertical dispersivities, respectively, $L$.
$\beta_1$, $\beta_2$, $\beta_3$ empirical coefficients.
$\gamma_1$, $\gamma_2$, $\gamma_3$ empirical coefficients.
$\theta$ porosity (liquid volume per porous medium volume), $L^3/L^3$.
$\theta_n$ volumetric content of NAPL.
$\nu$ kinematic viscosity, $L^2/t$.
$\Pi_1, \cdots, \Pi_6$ dimensionless variables defined in equations (35)–(40).
$\rho$ bulk density of the solid matrix, $M/L^3$.
$\tau$ tortuosity ($\tau \geq 1$).
$\phi$ arbitrary function.
$\Psi_i$ uniformity index.

**Abbreviations**

DNAPL dense nonaqueous phase liquid
NAPL nonaqueous phase liquid
TCE trichloroethylene

**Acknowledgments.** This work was sponsored by the Environmental Protection Agency, under award R-823579-01-0. The manuscript, however, has not been subjected to the Agency's peer and administrative review and therefore does not necessarily reflect the views of the Agency, and no official endorsement should be inferred. Additional support from the University of California, Irvine through an allocation of computer resources on the UCI SPP2000 is gratefully acknowledged.

## References

Abriola, L. M., T. J. Dekker, and K. D. Pennell, Surfactant-enhanced solubilization of residual dodecane in soil columns, 2, Mathematical Modeling, *Environ. Sci. Technol.*, *27*(12), 2341–2351, 1993.

Anderson, M. R., R. L. Johnson, and J. F. Pankow, Dissolution of dense chlorinated solvents into groundwater, 3, Modeling contaminant plumes from fingers and pools of solvent, *Environ. Sci. Technol.*, *26*(5), 901–908, 1992.

Bear, J., and A. Verruijt, *Modeling Groundwater Flow and Pollution*, D. Reidel, Norwell, Mass., 1987.

Bird, R. B., W. E. Stewart, and E. N. Lightfoot, *Transport Phenomena*, John Wiley, New York, 1960.

Borden, R. C., and C.-M. Kao, Evaluation of groundwater extraction for remediation of petroleum-contaminated aquifers, *Water Environ. Res.*, *64*(1), 28–36, 1992.

Borden, R. C., and M. D. Piwoni, Hydrocarbon dissolution and transport—A comparison of equilibrium and kinetic models, *J. Contam. Hydrol.*, *10*(4), 309–323, 1992.

Chrysikopoulos, C. V., Three-dimensional analytical models of contaminant transport from nonaqueous phase liquid pool dissolution in saturated subsurface formations, *Water Resour. Res.*, *31*(4), 1137–1145, 1995.

Chrysikopoulos, C. V., and K. Y. Lee, Contaminant transport resulting from multicomponent nonaqueous phase liquid pool dissolution in three-dimensional subsurface formations, *J. Contam. Hydrol.*, *31*(1–2), 1–21, 1998.

Chrysikopoulos, C. V., E. A. Voudrias, and M. M. Fyrillas, Modeling of contaminant transport resulting from dissolution of nonaqueous phase liquid pools in saturated porous media, *Transp. Porous Media*, *16*(2), 125–145, 1994.

Fried, J. J., P. Muntzer, and L. Zilliox, Ground-water pollution by transfer of oil hydrocarbons, *Ground Water*, *17*(6), 586–594, 1979.

Geller, J. T., and J. R. Hunt, Mass transfer from nonaqueous phase organic liquids in water-saturated porous media, *Water Resour. Res.*, *29*(4), 833–845, 1993.

Hoffman, J. D., *Numerical Methods for Engineers and Scientists*, 825 pp., McGraw-Hill, New York, 1992.

Holman, H.-Y. N., and I. Javandel, Evaluation of transient dissolution of slightly water-soluble compounds from a light nonaqueous phase liquid pool, *Water Resour. Res.*, *32*(4), 915–923, 1996. (Correction, *Water Resour. Res.*, *32*(6), 1917, 1996.)

Huyakorn, P. S., and G. F. Pinder, *Computational Methods in Subsurface Flow*, 473 pp., Academic, San Diego, Calf., 1983.

Illangasekare, T. H., J. L. Ramsey Jr., K. H. Jensen, and M. B. Butts, Experimental study of movement and distribution of dense organic contaminants in heterogeneous aquifer, *J. Contam. Hydrol.*, *20*(1–2), 1–25, 1995.

Imhoff, P. T., P. R. Jaffé, and C. F. Pinder, An experimental study of complete dissolution of a nonaqueous phase liquid in saturated porous media, *Water Resour. Res.*, *30*(2), 307–320, 1994.

Incropera, F. P., and D. P. DeWitt, *Fundamentals of Heat and Mass Transfer*, 3rd ed., 919 pp., John Wiley, New York, 1990.

International Mathematics and Statistics Libraries, *IMSL MATH/LIBRARY User's Manual*, version 2.0, Houston, Tex., 1991.

Johnson, R. L., and J. F. Pankow, Dissolution of dense chlorinated solvents into groundwater, 2, Source functions for pools of solvent, *Environ. Sci. Technol.*, *26*(5), 896–901, 1992.

Lee, K. Y., and C. V. Chrysikopoulos, Numerical modeling of three-dimensional contaminant migration from dissolution of multicom-

ponent NAPL pools in saturated porous media, *Environ. Geol*., *26*, 157–165, 1995.

Lee, K. Y., and C. V. Chrysikopoulos, NAPL pool dissolution in stratified and anisotropic porous formations, *J. Environ. Eng.*, *124*(9), 851–862, 1998.

Lee, K. Y., C. V. Chrysikopoulos, and T. C. Harmon, Measuring and modeling DNAPL pool dissolution in three-dimensional porous media, 1, Ideal pool geometry, in *Proceedings of the 1998 Symposium on Environmental Models and Experiments Envisioning Tomorrow* (*EnviroMEET '98*), edited by C. V. Chrysikopoulos, T. C. Harmon, and J. Bear, pp. 151–159, Univ. of Calif., Irvine, 1998.

Mackay, D. M., P. V. Roberts, and J. A. Cherry, Transport of organic contaminants in groundwater, *Environ. Sci. Technol*., *19*(5), 364–392, 1985.

Mayer, A. S., and C. T. Miller, The influence of mass transfer characteristics and porous media heterogeneity on nonaqueous phase dissolution, *Water Resour. Res*., *32*(6), 1551–1567, 1996.

Miller, C. T., M. M. Poirier-McNeill, and A. S. Mayer, Dissolution of trapped nonaqueous phase liquids: Mass transfer characteristics, *Water Resour. Res*., *26*(11), 2783–2796, 1990.

Parker, J. C., A. K. Katyal, J. J. Kaluarachchi, R. J. Lenhard, T. J. Johnson, K. Jayaraman, K. Ünlü, and J. L. Zhu, Modeling multiphase organic chemical transport in soils and groundwater, *Proj. CR-814230*, final report submitted to U.S. Environmental Protection Agency, Washington, D. C., 1991.

Perry, R. H., D. W. Green, and J. O. Maloney, *Perry's Chemical Engineers' Handbook*, 6th ed., McGraw-Hill, New York, 1984.

Pfannkuch, H. O., Determination of the contaminant source strength from mass exchange processes at the petroleum-groundwater interface in shallow aquifer systems, in *Proceedings of the NWWA Conference on Petroleum Hydrocarbons and Organic Chemicals in Groundwater*, pp. 111–129, Natl. Well Water Assoc., Dublin, Ohio, 1984.

Pinder, G. P., and L. M. Abriola, On the simulation of nonaqueous phase organic compounds in the subsurface, *Water Resour. Res*., *22*(9), 109S–119S, 1986.

Powers, S. E., C. O. Loureiro, L. M. Abriola, and W. J. Weber Jr., Theoretical study of the significance of nonequilibrium dissolution of nonaqueous phase liquids in subsurface systems, *Water Resour. Res*., *27*(4), 463–477, 1991.

Powers, S. E., L. M. Abriola, and W. J. Weber Jr., An experimental investigation of nonaqueous phase liquid dissolution in saturated subsurface systems: Steady state mass transfer rates, *Water Resour. Res*., *28*(10), 2691–2705, 1992.

Schincariol, R. A., F. W. Schwartz, and C. A. Mendoza, On the generation of instabilities in variable density flow, *Water Resour. Res*., *30*(4), 913–927, 1994.

Schwille, F., Groundwater pollution by minimal oil products, in *Proceedings of the Moscow Symposium*, *AISH Publ. 103*, pp. 226–240, Int. Assoc. of Sci. Hydrol., Gentbrugge, Belgium, 1975.

Schwille, F., *Dense Chlorinated Solvents in Porous and Fractured Media—Model Experiments*, translated from German by J. F. Pankow, Lewis, Boca Raton, Fla., 1988.

Seagren, E. A., B. E. Rittmann, and A. J. Valocchi, Quantitative evaluation of the enhancement of NAPL-pool dissolution by flushing and biodegradation, *Environ. Sci. Technol*., *28*(5), 833–839, 1994.

van der Waarden, M., A. L. A. M. Bridie, and W. M. Groenewoud, Transport of mineral oil components to groundwater, I, Model experiments on the transfer of hydrocarbons from a residual oil zone to trickling water, *Water Res*., *5*(2), 213–226, 1971.

Wang, H. F., and M. P. Anderson, *Introduction to Groundwater Modeling*, 237 pp., Academic, San Diego, Calif., 1982.

Weber, W. J., Jr., and F. A. DiGiano, *Process Dynamics in Environmental Systems*, John Wiley, New York, 1996.

Wilson, J. T., S. H. Conrad, E. Hagan, and W. R. Peplinski, The pore level spatial distribution and saturation of organic liquids in porous media, in *Proceedings of the NWWA Conference on Petroleum Hydrocarbons and Organic Chemicals in the Subsurface*, pp. 107–133, Natl. Well Water Assoc., Dublin, Ohio, 1988.

C. V. Chrysikopoulos and T.-J. Kim, Department of Civil and Environmental Engineering, University of California at Irvine, Irvine, CA 92697. (e-mail: costas@eng.uci.edu)

(Received June 10, 1998; revised October 9, 1998;
accepted October 9, 1998.)